Journal of Solid State Chemistry 182 (2009) 491–495

Contents lists available at ScienceDirect

Journal of Solid State Chemistry

journal homepage: www.elsevier.com/locate/jssc

Comparison of T-piece and concentric mixing systems for continuous flow synthesis of anatase nanoparticles in supercritical isopropanol/water

Lars L. Toft, David F. Aarup, Martin Bremholm, Peter Hald, Bo B. Iversen *

Centre for Energy Materials, Department of Chemistry and iNANO, University of Aarhus, Langelandsgade 140, DK 8000 Aarhus, Denmark

ARTICLE INFO

Article history:
Received 24 August 2008
Received in revised form
31 October 2008
Accepted 12 November 2008
Available online 21 November 2008

Keywords:
Supercritical fluids
Nanoparticles
Mixing geometry
Absolute crystallinity
Size distributions

ABSTRACT

T-piece and concentric counter-flow mixing systems are compared in continuous flow supercritical solvothermal synthesis of TiO_2 at identical system parameters. The phase pure anatase nanoparticle products were characterized with powder X-ray diffraction (PXRD), transmission electron microscopy (TEM) and small angle X-ray scattering (SAXS), and the particle size, size distribution and absolute crystallinity mapped as a function of temperature, precursor concentration, flow rate and pressure for the two different continuous flow reactors. The particles synthesized with the T-piece geometry are smaller with a narrower size distribution, possibly indicating a more effective mixing, than particles synthesized at the same conditions with concentric counter-flow geometry. In general, an increased synthesis temperature leads to an increase in absolute crystallinity. For the particles synthesized with the concentric reactor geometry crossing of the critical point of the solvent causes a decrease in the particle size and size distribution, and conditions just above the critical temperature are demonstrated to be optimal for continuous solvothermal synthesis of anatase.

1. Introduction

In recent years continuous flow synthesis close to the critical point of the solvents has been shown to be advantageous for the production of nanoparticles [1–3]. The produced nanoparticles have a narrow size distribution due to the high nucleation rate obtained when the supercritical solvent is mixed with cold reactant [4–7]. In the numerous reports on synthesis of nanoparticles using continuous flow supercritical reactors, the preferred mixing geometry has been the T-piece, which allows flexible instrument design [8,9]. However, since the exact mixing of the solvents influences the product characteristics and reactor performance, it is clearly of interest to optimize the reactor design for specific applications. Lester et al. performed numerical simulations of different mixing geometries and developed the counter-flow concentric geometry (nozzle reactor) [10]. Here, we present the first direct experimental comparison between the T-piece and concentric counter-flow mixing geometries.

In synthesis of TiO_2, the products consist of phase pure anatase [11] and the particle characteristics are easily tuned due to the changes in solubility around the critical point [12]. This makes the technique suitable for tailoring the product characteristics. TiO_2 has found use in many different areas such as solar cells, gas sensors, photocatalysts and as corrosive resistant coatings [13]. It is well known that the particle size and morphology influence the photocatalytic efficiency [14]. One of the less discussed aspects is the absolute crystallinity, which is also crucial to obtain an effective photocatalyst [14,15]. In the present study the absolute crystallinity is determined for all products to bring more attention to this aspect of titania nanoparticle synthesis.

The conventional sol–gel method produces small particles, but often requires post-treatment in order to achieve highly crystalline products and is performed as a batch process. Furthermore, the sol–gel technique is time-consuming and the produced particles have a wide size distribution [4]. From in-situ synchrotron studies of supercritical sol–gel reactions, it has been established that the nanoparticle formation and growth phases progress as in the conventional sol–gel reactions but the synthesis time is reduced from hours to minutes [16,17]. The fast kinetics of the supercritical solvothermal reaction makes it possible to obtain fully crystalline products in a continuous synthesis [4].

One aim of the present study is to compare the T-piece (Fig. 1A) and the concentric geometries (Fig. 1B) under identical experimental conditions. This is done by producing nanoparticles with the same synthesis parameters in the two different setups. Producing comparable synthesis conditions is in itself a major challenge since the heating in the two configurations differ. In fact it is quite difficult to compare studies carried out on different synthesis reactors due to differences in dimensions, heating, flow, etc. To reduce this problem the reported temperatures in the present study are measured inside the reactor at the mixing point and they do not refer e.g. to the set point of the external heater

* Corresponding author. Fax: +45 8619 6199.
E-mail address: bo@chem.au.dk (B.B. Iversen).

0022-4596/$ - see front matter © 2008 Elsevier Inc. All rights reserved.
doi:10.1016/j.jssc.2008.11.009

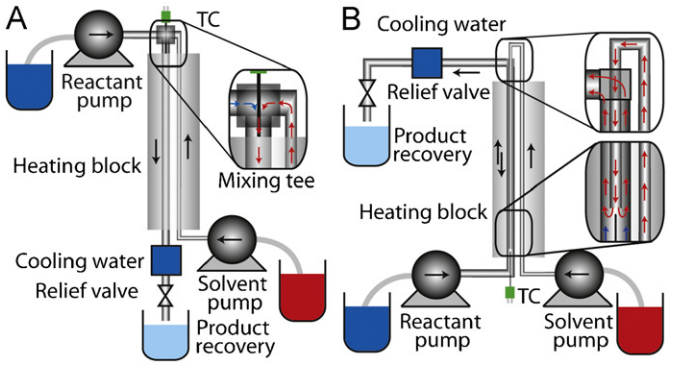

Fig. 1. Schematic outline of the two experimental designs, where (A) is T-piece geometry and (B) is the concentric geometry.

arrangement. The comparison of the particle products is carried out by comprehensive characterization using powder X-ray diffraction (PXRD), transmission electron microscopy (TEM) and small angle X-ray scattering (SAXS). While TEM and PXRD are widely used in the supercritical synthesis literature, it is still not common to use SAXS. This technique is complementary to TEM and PXRD, and here it provides not only particle size estimates, but also estimates of size distributions that are inherently representative for the entire synthesis products.

2. Experimental

The supercritical synthesis was performed using two different setups, Fig. 1. Both reactors were constructed in stainless steel 316 using 3/8 in tubes (outer diameter 9.6 mm and inner diameter 7.5 mm) and Swagelok adaptors. For the concentric reactor design (Fig. 1B), the internal tube was 1/8″ (3.2 mm outer diameter and 2.0 mm inner diameter). Heating was obtained with a 20 cm long aluminum heating block with 10 cartridge heaters (total power 1400 W), which is in direct contact with the steel tubes. The heated volumes of the two reactors are thus 8.8 and 8.2 ml for the T and concentric reactor geometry, respectively. A thermocontroller (Cal 9400) was used to control the heating block temperature, while several other thermocouples were used to monitor the internal reactor temperature at different positions. Two pneumatic metering pumps (Williams Milton Roy P250V225) were used to deliver the reactant and solvents streams. In both reactors continuous mixing of preheated isopropanol containing 5.0 vol% water (solvent) and cold titanium tetraisopropoxide (reactant, TTIP) was used to produce phase pure anatase nanoparticles by hydrolysis followed by condensation [5]. By keeping the synthesis parameters equal for the two different systems, the role of the mixing system was evaluated. The reactant (TTIP) was kept at room temperature until mixing with the preheated solvent in order to obtain a very high heating rate, which results in instantaneous and well controlled production of anatase particles at the mixing point. After the streams have reacted the products are cooled by an external water jacket and finally depressurized and recovered.

The temperature was measured at the mixing point for both geometries, and furthermore a thorough temperature profile was measured for the concentric mixing system. In the temperature analysis for the concentric reactor isopropanol was used in both the reactant and the solvent strings, and the system parameters were held constant at: $P = 280$ bar, flow rate = 5 ml/min (each pump), and block temperature = 375 °C. By translation of an internal thermocouple the reaction temperature profile was mapped out. The thermal gradients in the two reactors are different due to the fact that the two concentric reactor tubes are in thermal contact. The counter-flow in the concentric tubes has some similarity to the principle in a heat exchanger and when the mixing point temperature is kept identical for the two geometries, the final reaction temperature in the concentric reactor will be somewhat lower than in the T-reactor.

PXRD data was measured with a Stadi P STOE diffractometer using monochromatic Cu$K\alpha_1$ radiation (Ge(111) monochromator). The volume weighted crystallite sizes were determined using the Scherrer equation, $D = K\lambda/(\mathrm{FWHM}\cos(\theta))$ with K equal to 0.94. Correction for the instrumental broadening was performed with the method developed by Wertheim et al. [18]. The instrumental broadening was obtained from the peak-width of a LaB_6 standard sample. For the anatase phase the (101) peak was fitted with a pseudo-Voigt function to obtain the FWHM. The absolute crystallinity was determined by mixing of the samples with fully crystalline CaF_2 powder in a precisely determined mass fraction close to 50 wt%. Afterwards the ratio of the integrated peak intensity of the most intense peak for each phase was compared with the value obtained from a sample containing pure 100% crystalline anatase (a crushed anatase single crystal) mixed with CaF_2.

SAXS data was measured on a Bruker AXS Nanostar. The *as prepared* isopropanol suspended products were loaded into

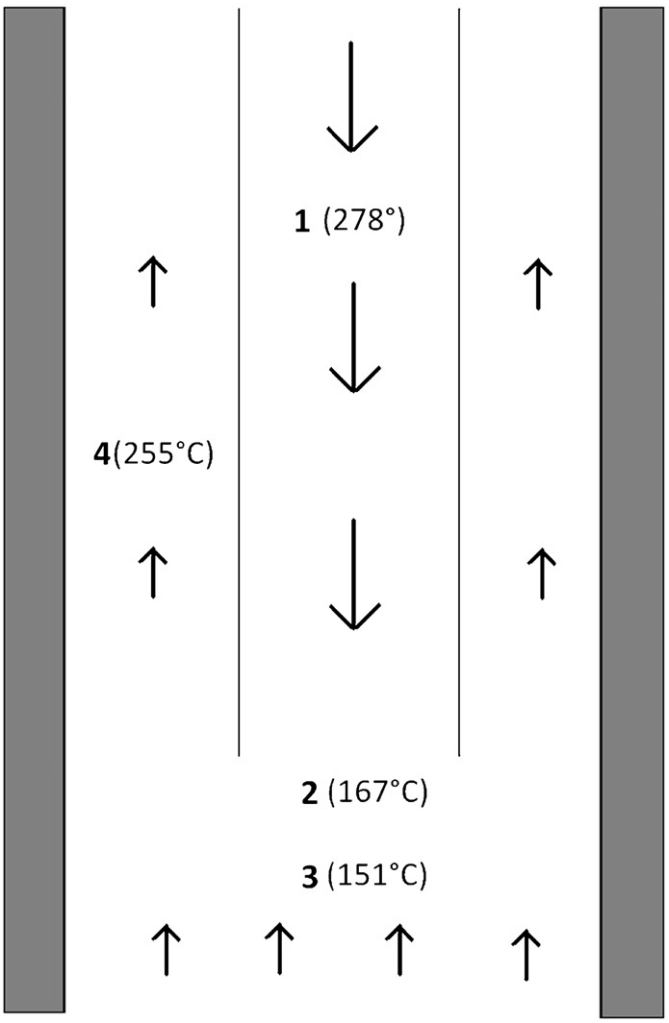

Fig. 2. The four different positions used for temperature analysis in the concentric geometry with a heating block temperature of 375 °C. The thermocouple was placed (1) 7.3 cm above the mixing point (MP), (2) at the MP, (3) 0.9 cm below MP, and (4) 6.1 cm above MP.

borosilicate capillaries (inner diameter 2.0 mm) flame-sealed and then placed in a vacuum chamber for measurement. A reference capillary containing pure isopropanol was measured for background subtraction. The data were modeled as polydisperse hard-spheres [19] using a Schulz-Zimm size distribution function [20].

TEM images (Phillips CM20 200 kV) were recorded for selected samples. The *as prepared* products were diluted with isopropanol (1000 times) and deposited on carbon coated TEM grids by evaporation of the solvent at room temperature. Size distributions were determined from TEM images by manual counting.

Thermogravimetric and differential thermal analysis (TG/DTA) was carried out on a Netzsch STA 449C Jupiter in order to determine the mass of the solvent and organic residues in the samples. Data were recorded up to 900 °C using a ramp of 10 °C/min and an argon atmosphere with a flow rate of 40 ml/min.

Fourier transform infrared spectroscopy (FTIR) measurements were made on a Perkin-Elmer Paragon 1000 to estimate the content of organic residues in the products.

3. Results and discussion

Temperature analysis was performed for the concentric geometry using a movable internal thermocouple placed in different positions. The temperature data, Fig. 2, show that the difference between the mixing temperature (position 2) and the temperature of the preheated solvent (position 1) is 111 °C. Furthermore, the difference between the mixing temperature and the heating block temperature is up to ~200 °C in the concentric geometry (Fig. 2) and up to ~250 °C in the T-piece geometry (data not shown). Thus, even in experiments with steel tubes and a large heating reservoir, the heat transfer to the solvent is not optimal. The mixing temperatures in the two setups with identical system parameters (block temperature, pressure and flow rate) are also very different. A block temperature of 425 °C resulted in a mixing temperature of 265 °C at the concentric setup and 164 °C at the T-piece. It is somewhat surprising that the temperature difference between the heating block and the solvent is of such large magnitude, and the result questions whether studies reported in the literature in general have been performed under supercritical conditions. The temperature analysis highlights that not only is the mixing geometry different but also the temperature profile is different between the concentric and the T-piece geometries after mixing.

In Table 1 the experimental conditions, crystallite size, particle size, particle size distribution and absolute crystallinity estimates are summarized. The table provides volume averaged size estimates for the crystallites (WAXS) and particles (SAXS), respectively. The sizes obtained using the Scherrer equation are volume averaged crystallite sizes. Normally, sizes determined from SAXS data are reported as either (average) radius of gyration or as number averaged particle size estimates, but to provide a direct comparison with the PXRD data we calculate the volume weighted average size from the number averaged size distribution from SAXS modeling using the procedure described by Becker et al. [7]. For completeness, we have also characterized potential organic residues on the particles using TG/DTA and FTIR. The TG/DTA measurements of two representative samples showed mass losses of 10±2%, mainly due to loss of physisorbed solvent (8±1% at 100–300 °C) but also due to decomposition of chemisorbed organic species (2±1% at 300–500 °C). The FTIR-spectra showed the expected Ti–O–Ti stretch mode at 600–400 cm^{-1} and the Ti–OH stretch mode at 1600 and 3400 cm^{-1}. Furthermore, the FTIR-spectra showed a small peak at 2900 cm^{-1} due to C–H stretching, indicating a low content of organic residues [21].

The influence of the mixing temperature for the two mixing geometries is evaluated by comparing experiments where the flow rate, concentration and pressure are kept constant at 5 ml/min,

Table 1
Experimental conditions and anatase product characteristics.

Geometry	Flow rate (ml/min)	Pressure (bar)	T_{mix} (°C)	C(TTIP) (M)	$\langle D\rangle_{vol}$ (WAXS) (nm)	$\langle D\rangle_{vol}$ (SAXS) (nm)	Crystallinity (%)	σ (nm)
Concentric	5.0	280	139±4	0.10	13.0±0.2	12.4±0.2	28.2±2.0	1.74±0.02
	5.0	280	160±1	0.10	14.1±0.2	15.0±1.1	74.2±2.0	2.11±0.03
	5.0	280	168±1	0.10	15.0±0.1	15.4±0.9	77.8±2.1	2.20±0.02
	5.0	280	178±1	0.10	15.4±0.1	15.6±0.7	76.3±2.0	2.26±0.02
	5.0	280	212±1	0.10	14.0±0.1	14.6±0.3	85.7±2.3	1.95±0.02
	5.0	280	227±2	0.10	14.7±0.1	15.4±0.3	84.5±2.2	1.98±0.03
	5.0	280	250±4	0.10	15.6±0.1	16.1±0.3	98.1±2.6	2.03±0.04
	5.0	280	265±3	0.10	16.7±0.1	16.8±0.3	77.8±2.1	2.11±0.04
	5.0	280	228±2	0.05	13.4±0.1	14.2±0.3	86.5±2.3	1.95±0.02
	5.0	280	229±2	0.10	14.5±0.1	15.0±0.3	101.1±2.7	2.03±0.02
	5.0	280	233±2	0.25	16.0±0.1	17.6±0.7	94.1±2.5	2.53±0.02
	5.0	280	228±2	0.10	14.6±0.1	15.0±0.3	101.1±2.7	2.03±0.02
	7.5	280	235±2	0.10	13.8±0.1	13.9±0.6	84.7±2.2	2.10±0.01
	9.0	280	233±2	0.10	12.1±0.2	14.1±3.8	49.0±1.3	1.84±0.16
	5.0	272	228±3	0.10	14.7±0.1	15.4±0.3	84.5±2.2	1.98±0.03
	5.0	200	229±1	0.10	14.6±0.1	14.6±0.4	85.9±2.3	1.99±0.03
	5.0	102	222±1	0.10	14.0±0.1	13.4±0.9	82.1±2.2	1.93±0.02
T-piece	5.0	280	134±1	0.10	11.0±0.2	11.2±1.7	33.0±2.2	1.33±0.09
	5.0	280	140±1	0.10	12.3±0.1	11.9±0.3	47.6±3.2	1.52±0.01
	5.0	280	154±3	0.10	12.9±0.1	12.7±0.7	73.1±4.9	1.83±0.01
	5.0	280	156±1	0.10	13.0±0.1	13.3±0.6	80.4±5.3	1.91±0.01
	5.0	280	164±1	0.10	13.3±0.1	13.7±0.6	104.4±6.9	1.97±0.01
	5.0	300	138±1	0.05	11.2±0.1	11.5±0.9	73.6±4.9	1.65±0.02
	5.0	300	143±1	0.10	10.6±0.1	11.9±0.5	55.8±3.7	1.71±0.01
	5.0	300	161±4	0.25	11.4±0.3	12.7±0.4	25.5±1.7	1.82±0.01
	5.0	280	140±2	0.10	13.8±0.1	14.1±0.9	86.8±4.6	2.01±0.02
	9.0	280	142±4	0.10	9.8±0.4	12.2±0.6	3.6±2.3	1.64±0.02

T_{mix} is the measured temperature at the mixing point, C(TTIP) is the precursor concentration, $\langle D\rangle_{vol}$ (WAXS) is the volume averages crystallite size obtained from the Scherrer equation (corrected for instrumental broadening), $\langle D\rangle_{vol}$ (SAXS) is the *volume* averaged particle size obtained from SAXS and σ is a measure of the width of the particle size distribution.

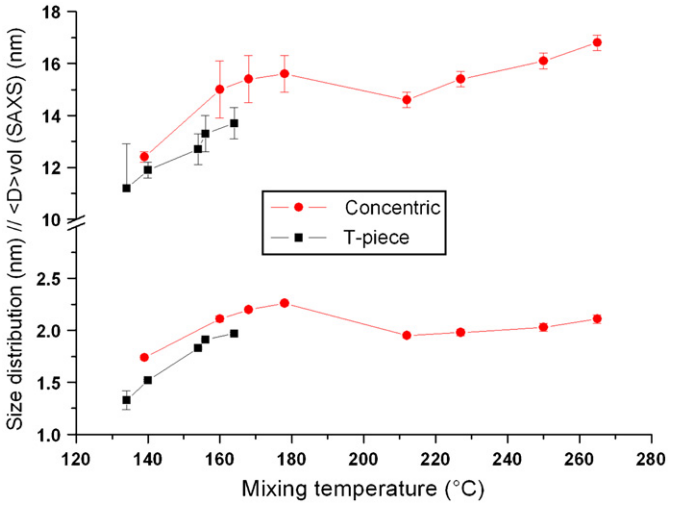

Fig. 3. The temperature dependence of the volume weighted particle size (top) and size distribution width (bottom) both determined by SAXS. The red spheres refer to the concentric mixing and black squares to the T-piece mixing.

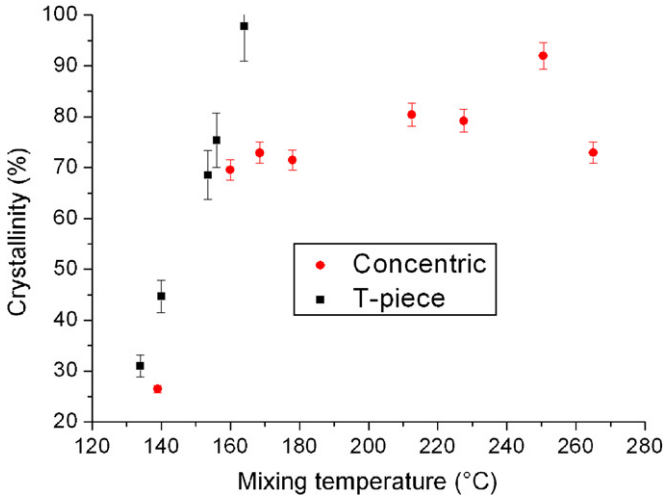

Fig. 4. Temperature dependence of the absolute crystallinity for the two different geometries.

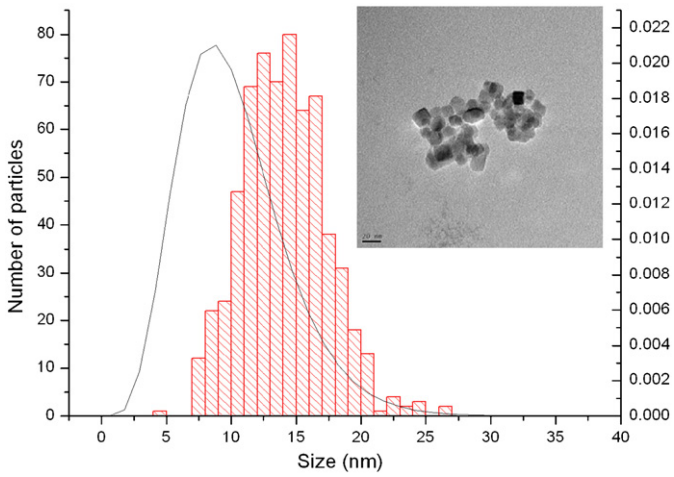

Fig. 5. Comparison of the number averaged size distributions determined from SAXS and TEM.

0.10 M and 280 bar, respectively. As seen in Fig. 3 the particle size increases as the temperature increases, but there is a sudden drop in both particle size and the width of the particle size distribution (σ-value) for the concentric reactor at a mixing temperature between 180 and 205 °C. Since further heating takes place after the mixing point this drop matches the transition from sub- to supercritical isopropanol ($P_C = 65$ bar, $T_C = 235$ °C). As described above there is a big difference between the block temperature and the mixing temperature in the T-piece system, and this configuration restricted synthesis in the supercritical regime due to the temperature limit of the aluminum heating block. Furthermore, the more intense heating after mixing in the T-piece reactor did not allow higher temperatures because the isopropanol decomposes. The decrease in solubility and viscosity around the critical point is responsible for the drop in particle size [12]. Furthermore, Ostwald ripening is not pronounced in the supercritical phase [8].

The data in Table 1 reveal that pressure does not have a significant effect on the synthesized particles, and there is thus no benefit of performing the reaction far above the critical pressure. Increasing the flow rate lowers the particle size and size distribution, but also the crystallinity. However, the flow rate is closely related to the temperature, which is clearly seen to influence the characteristics of the particles. By increasing the flow rate the heating of the product is reduced and this results in smaller particles. Furthermore, the residence time in the reactor is lowered, and the particles do not grow to the same extent. Increase of the reactant concentration is found to increase both the particle size, and higher concentration also increases the width of the size distribution. The temperature dependence on the crystallinity is plotted in Fig. 4. It is observed that an increase in temperature leads to a clear increase in the crystallinity. An analogy can be drawn to the effect of post-calcination of TiO_2 samples, which is normally required to obtain a high crystallinity with other preparation techniques [22]. The two mixing geometries have quite different temperature dependencies for the crystallinity. Thus, there is a very strong increase in the crystallinity with increasing mixing temperature for the T-piece, whereas the concentric geometry appears to reach a maximum value of about 90% after an initial strong increase. This indicates that the T-piece reactor has a more effective heating after the initial nucleation of the crystallites.

In an industrial context the reproducibility of a given synthesis is important. In the present case the reproducibility can be tested by comparing two points with similar conditions such as the sixth and the tenth syntheses for the concentric geometry in Table 1. In both cases the flow rates were 5 ml/min, the pressure 280 bar, the precursor concentration 0.10 M and the mixing temperature 227–229 °C. In both cases the particle size is around 15 nm, but in synthesis 6 the crystallinity of the particles is 84.5%, whereas it is 100% in synthesis 10. This indicates that the "state of the reactor", i.e. the length of the synthesis run, the amount of particles that have deposited on the inner surface, the temperature fluctuations, etc. are parameters that could influence the product outcome. Therefore comparison of specific synthesis runs can be difficult, and it may be more appropriate to compare trends. Nevertheless, comparison of the particle sizes from the two different mixing systems (e.g. 139 ± 4 °C for concentric and 140 ± 1 °C for the T-piece system) shows that in general the largest particles are synthesized with the concentric reactor. The heating of the products before cooling and recovery is dissimilar, which could hinder any conclusion. However, the post-heating in the T-piece system is actually more intense than in the concentric configuration, and this should give a further increase in particle size and crystallinity. Therefore it can be concluded that the T-piece mixing results in smaller particles while maintaining a

high crystallinity. This indicates that the T-piece mixing geometry produces a more effective mixing of the reactant and solvent.

The TEM image in Fig. 5 shows isotropic particles with 90° facets as expected for tetragonal anatase nanoparticles with a high degree of crystallinity. The particle diameter measured by TEM is also shown in Fig. 5 together with the size distribution obtained from SAXS. The shape of the curves match very well confirming the choice of the Schultz-Zimm distribution, but the particles sizes obtained with TEM are significantly larger. This could be explained by a lack of resolution for the smallest particles and the fact that aggregated particles overlap, which also tends to blur the smaller particles. The volume weighted particle sizes estimated by PXRD and SAXS have shown good agreement (Table 1). The size determined from SAXS is in many cases slightly larger than the PXRD value, but this difference can be explained by the limited crystallinity of the particles. The SAXS technique measures the particle size including both crystalline and amorphous phases.

4. Conclusion

A thorough evaluation of the synthesis parameter space (temperature, precursor concentration, flow rate, pressure) has been performed for supercritical synthesis of anatase nanoparticles using the two different mixing geometries. All products were extensively characterized using PXRD, SAXS, TEM, TGA/DTA and FTIR. Absolute crystallinity is a key parameter in applications of anatase particles. Highly crystalline particles were produced (in some cases 100%) which means that calcination of the products is redundant for supercritical synthesis. Phase pure anatase can be produced with short reaction times and with good control over particle size and crystallinity. The study provides a clear experimental verification that when crossing the critical point there is a drop in particle size. Another important factor in the synthesis is "the state of the reactor", which affects the formed particles thereby making exact reproducibility difficult. Mapping of the temperature profile inside the reactor has revealed that there are large differences between the heating block temperature and the temperature of the solvent even for a system using steel tubes and a large heating reservoir. This suggests that some studies may not be carried out under truly supercritical conditions. Comparison between T-piece and concentric reactor geometries shows that smaller and more crystalline particles are obtained with the T-piece, and this indicates a more effective mixing in this setup.

References

[1] E. Reverchon, R. Adami, J. Supercrit. Fluids 37 (2006) 1–22.
[2] P. Boldrin, A. Hebb, A. Chaudhry, L. Otley, B. Thiebaut, P. Bishop, J. Darr, Ind. Eng. Chem. Res. 46 (2007) 4830–4838.
[3] C. Xu, A. Teja, J. Supercrit. Fluids 44 (2008) 85–91.
[4] P. Hald, J. Becker, M. Bremholm, J.S. Pedersen, J. Chevallier, S.B. Iversen, B.B. Iversen, J. Solid State Chem. 179 (2006) 2674–2680.
[5] T. Adschiri, K. Kanazawa, K. Arai, J. Am. Ceram. Soc. 75 (1992) 1019–1022.
[6] T. Adschiri, K. Kanazawa, K. Arai, J. Am. Ceram. Soc. 75 (1992) 2615–2618.
[7] J. Becker, P. Hald, M. Bremholm, J.S. Pedersen, J. Chevallier, S.B. Iversen, B.B. Iversen, ACS Nano 2 (2008) 1058–1068.
[8] T. Adschiri, Y. Hakuta, K. Sue, K. Arai, J. Nanopart. Res. 3 (2001) 227–235.
[9] K. Sue, K. Murata, K. Kimura, K. Arai, Green Chem. 5 (2003) 659–662.
[10] E. Lester, P. Blood, J. Denyer, D. Giddings, B. Azzopardi, M. Poliakoff, J. Supercrit. Fluids 37 (2006) 209–214.
[11] H. Hayashi, K. Torii, J. Mater. Chem. 12 (2002) 3671–3676.
[12] T. Adschiri, Y. Hakuta, K. Arai, Ind. Eng. Chem. Res. 39 (2000) 4901–4907.
[13] U. Diebold, Surf. Sci. Rep. 48 (2003) 53–229.
[14] J. Porter, Y. Li, C. Chan, J. Mater. Sci. 34 (1999) 1523–1531.
[15] M. Inagaki, R. Nonaka, B. Tryba, A. Morawski, Chemosphere 64 (2006) 437–445.
[16] H. Jensen, M. Bremholm, R.P. Nielsen, K.D. Joensen, J.S. Pedersen, H. Birkedal, Y.-S. Chen, J. Almer, E.G. Søgaard, S.B. Iversen, B.B. Iversen, Angew. Chem. Int. Ed. 46 (2007) 1113–1116.
[17] M. Bremholm, H. Jensen, S.B. Iversen, B.B. Iversen, J. Supercrit. Fluids 44 (2008) 385–390.
[18] G. Wertheim, M. Butler, K. West, D. Buchanan, Rev. Sci. Instrum. 45 (1974) 1369–1371.
[19] J. Pedersen, J. Appl. Cryst. 27 (1994) 595–608.
[20] J. Pedersen, Adv. Colloid Interface Sci. 70 (1997) 171–210.
[21] Y.F. Chen, C.Y. Lee, M.Y. Yeng, H.T. Chiu, J. Cryst. Growth 247 (2003) 363–370.
[22] C.H. Liang, Y. Shimizu, T. Sasaki, N. Koshizaki, J. Mater. Res. 19 (2004) 1551–1557.